Mon. Not. R. Astron. Soc. **382,** 609–620 (2007) doi:10.1111/j.1365-2966.2007.12287.x

η Muscae: a young detached binary with two identical components

V. Bakış,[1]★ H. Bakış, Z. Eker and O. Demircan
Çanakkale Onsekiz Mart University Observatory, Terzioğlu Campus, TR-17040, Çanakkale, Turkey

Accepted 2007 July 26. Received 2007 July 26; in original form 2007 May 8

Downloaded from https://academic.oup.com/mnras/article/382/2/609/1028017 by Akdeniz University user on 20 September 2021

ABSTRACT

High-resolution ($\lambda/d\lambda \sim 41\,000$) echelle spectra of the multiple system η Muscae were analysed. Precise spectroscopic orbital elements of the close pair η Muscae-A were obtained by means of two techniques; cross-correlation and spectral disentangling. The updated light elements of the close pair were derived using new photometric and spectroscopic data together with *Hipparcos* ephemerides. According to simultaneous studies of radial velocities with *Hipparcos* light curve and recent and historic light curves in Strömgren bands, η Mus-A consists of two quasi-identical components: $M_1 = 3.30\,M_\odot, M_2 = 3.29\,M_\odot, R_1 = 2.14\,R_\odot$, $R_2 = 2.13\,R_\odot, T_1 = 12\,700$ K and $T_2 = 12\,550$ K separated from each other by $a = 14.11\,R_\odot$ in an orbit inclined 77°.4. The membership of η Mus-A to the Lower Centaurus–Crux OB association is discussed. The rotational velocity of the primary component was found to be smaller than that of the secondary component. The asynchronous slow rotation of the primary and the synchronous rotation of the secondary imply a recent decrease in the orbital period, either due to orbital angular momentum being transferred to the visual companion η Mus-C or due to relatively frequent stellar encounters in this crowded region. The visual companion η Mus-B is found to be gravitationally unbound to the close pair η Mus-A. The radial velocity measurements of the visual companion η Mus-B, when combined with its positional information, support its membership to the Lower Centaurus–Crux OB association, but the evidence for membership of η Mus-A is weaker.

Key words: binaries: general – stars: kinematics – stars: individual: η Muscae – techniques: photometric – techniques: radial velocities – techniques: spectroscopic.

1 INTRODUCTION

The bright southern binary system η Muscae (HD 114911, Hip64661, $V \sim 4.78$ mag, $P \sim 2.40$ d) is one of the eclipsing binary stars discovered during the *Hipparcos* survey (ESA 1997). The trigonometric parallax of the system, as obtained by *Hipparcos*, is 8.04 mas. There were several studies (e.g. Schilt & Jackson 1949; Eggen & Lyngå 1968; Crawford, Barnes & Golson 1970; Lindroos 1983; van Paradijs et al. 1986; Slawson, Hill & Landstreet 1992) which discussed the brightness and colours of η Mus. Moffat & Seggewiss (1977) noted the photometric variations of η Mus-A during their narrow-band photometric observations of the Wolf–Rayet binary θ Mus. The small number of observations did not allow them to derive a unique period; instead, they suggested a number of possible periods including the true one.

In the catalogue of multiple stars (Tokovinin 1997), η Mus is listed with a common proper motion visual companion, η Mus-B, at 60 arcsec from η Mus-A at a position angle of 332°. η Mus-B is 3.4 mag fainter than η Mus-A. Later, Medici & Hubrig (2000) reported that the triple system η Mus is actually a quadruple system. Details of the quadruple system were later given by Hubrig et al. (2001). The fourth component, η Mus-C, which is separated by 2.71 arcsec at a position angle of 125°, was announced to be 5.25, 4.54 and 3.32 mag dimmer than η Mus-A in J, H and K bands, respectively, and claimed to be a pre-main sequence (PMS) object with a mass of $0.88\,M_\odot$ and effective temperature of $T_{\rm eff} = 4900$ K.

Slawson et al. (1992) compiled *UBV* photometric measurements of a large number of B- and A-type stars, including η Mus-A, in a sky region containing Sco–Cen. $U - B$ and $B - V$ colours of η Mus-A in this list (−0.36, −0.09) imply a colour temperature of 12 700 K, which is consistent with the effective temperature of 12 760 K determined by Hubrig et al. (2001) using Geneva photometry. However, using spectrophotometric data and referring to the drop between the Balmer and the Paschen continuums (Balmer jump), Sokolov (1995) gave a rather different effective temperature of $16\,130 \pm 960$ K.

According to de Zeeuw et al. (1999), η Mus-A is given ∼60 per cent probability of being a member of Scorpio–Centaurus (or Sco OB). Sco OB is the OB association nearest to the Sun, which is believed to be ∼16–20 Myr old (Sartori, Lepine & Dias 2003).

★E-mail: bakisv@comu.edu.tr

© 2007 The Authors. Journal compilation © 2007 RAS

On the other hand, if η Mus-A is a member of Sco OB, then it is expected to be an order of magnitude younger than the age which is estimated by Hubrig et al. (2001). Clarification of membership, therefore, seems to be important in understanding η Mus-A itself and also because the characteristics of the binary population in OB associations, such as Sco–Cen OB, will furnish a better understanding of the star formation process (Brown 1999).

Spectral-line variations of η Mus-A were first noted by Campbell (1928). From spectra obtained later, Buscombe & Morris (1961) derive 20-d orbital period from its radial velocity (RV) curve with a semi-amplitude of 56.5 km s^{-1} as a single-lined system. Tokovinin (1997) estimated the mass of the primary $M_1 = 4.48\,\mathrm{M}_\odot$ according to its spectral type. From the mass function of the single-lined system, a mass of $M_2 = 2.63\,\mathrm{M}_\odot$ was claimed for the unseen secondary. Giuricin, Mardirossian & Mezzetti (1984) used these incorrect orbital elements of η Mus-A in their statistical study about period distributions among the close binary systems. η Mus-A is recorded in the 'Catalogue of the Orbital Elements of Spectroscopic Binary Systems: 8' (Batten, Fletcher & MacCarthy 1989) with the same incorrect orbital elements proposed by Buscombe & Morris (1961).

The double-lined character of η Mus-A spectra was first noted during a study of the λ 3984 Å feature in late-B type spectroscopic binaries by Hubrig & Mathys (1996). After the discovery of the eclipsing nature of η Mus-A by nearly equal minima by *Hipparcos*, Hensberge et al. (2003) confirmed the photometric period found by *Hipparcos* and claimed that the 20-d period proposed by Buscombe & Morris (1961) is spurious. Although the mass ratio of η Mus-A is estimated to be $M_1/M_2 = 1.14$ by Hensberge et al. (2003), the renewed spectroscopic orbital elements have not been announced.

In this study, we analyse the double-lined spectra. The RVs derived in this paper imply that the components of η Mus have nearly equal masses. New orbital parameters have been determined. The membership of the η Mus-A system to the Lower Centaurus–Crux (LCC) OB association is also discussed.

2 OBSERVATIONS AND DATA REDUCTION

2.1 Spectroscopy

The spectra of η Mus-A and η Mus-B were taken by the High Efficiency and Resolution Canterbury University Large Echelle Spectrograph (HERCULES) of the Department of Physics and Astronomy, University of Canterbury, New Zealand. It is a fibre-fed echelle spectrograph, attached to the 1-m McLellan Telescope at the Mt John University Observatory (MJUO), near Lake Tekapo ($\sim 43^\circ 59^\mathrm{m}$ S, $174^\circ 27^\mathrm{m}$ E). The spectrograph is mounted on a stable optical bench and enclosed within a vacuum vessel located in a thermally insulated room. Light from the Cassegrain focus can be fed to the spectrograph using a 20 m length of optical fibre of selectable cross-section (Hearnshaw et al. 2002). The spectrograph is designed to provide continuous wavelength coverage from $\lambda = 380$ to 880 nm in over 80 echelle orders. Two resolving powers of $R = 41\,000$ and 70 000 are possible to obtain high-precision spectroscopic observations of a variety of objects over extended times. Choices of resolving powers are made possible by selecting one of three optical fibres with different sizes. Fibre 1, which is a 100-μm fibre without slit giving a moderately high resolving power of 41 000, has been selected for the observations of this project. The angular size of the fibre core projected on to the sky ($\theta \sim 4.5$ arcsec) is not less than the median seeing at MJUO which was reported to be about 3.5 arcsec (Hearnshaw et al. 2002). Fibres 2 and 3 have a resolving power of $R = 70\,000$ but require good seeing conditions ($\theta \sim 2$ arcsec). A more detailed description of the spectrograph can be found in Hearnshaw et al. (2002) and Skuljan, David & Hearnshaw (2004).

A total of 52 spectra (50 for η Mus-A, two for η Mus-B) have been collected in two different observing sessions. The log of observations is given in Table 1 together with RVs obtained in Section 3.

In the first observing session, 43 spectra of η Mus-A have been collected over four nights (2006/05/17–20) using a SITe CCD with 1024×1024 pixels of 24 μm. Four CCD positions are required to achieve complete spectral coverage. Position 2 ($\lambda\lambda \sim 4500$–7200 Å) has been preferred because spectral-line density, continuum flux and CCD efficiency are then optimized for this study with this position. A typical 160 s of exposure time gave an average signal-to-noise ratio (S/N) = 130 in the 550-nm region in the extracted continuum. In the second session, nine spectra (seven of η Mus-A and two of η Mus-B) have been collected over three nights (2006/08/19 and 20 and 2006/09/07) with a new 4×4 k Spectral Instruments 600 series (SI600s) CCD camera. The pixel size is 15 μm and the detector covers the complete spectral range from around 3650 to 9400 Å. An average S/N of 90 in the 550-nm region was achieved with a typical exposure time of 290 s.

For all observations, comparison spectra of a Thorium–Argon arc lamp were recorded before and after each exposure. The dispersion solution was interpolated between the two thorium spectra for the exact time of the stellar observation, which is a flux-weighted mean obtained from the exposure metre readings during the observation. A set of white lamp images was taken every night for flat-fielding.

All spectra of the different components of η Mus and the template stars were reduced in a consistent way with the HERCULES REDUCTION SOFTWARE PACKAGE (HRSP) developed in the department of Physics and Astronomy, University of Canterbury. The procedure of reduction is a standard for echelle spectra (Skuljan 2004).

When normalizing the raw spectra extracted from CCD images, a second- or third-order polynomial was fitted on the selected parts of the continuum. The spectra are normalized by dividing the spectra by the fitted polynomial. Telluric lines, mostly water, were removed especially at the echelle order 97 where He I 5875 is located, using a sample spectrum of the rapidly rotating early-type star HD 151676 (A3V) taken in the same observing run. A scalefactor modifying the strength of the telluric lines was adjusted for each spectrum of η Mus. Telluric line contamination is negligible in other echelle orders that were used in this study.

2.2 Light elements

The light elements of η Mus-A according to *Hipparcos* photometry are

$$\mathrm{HJD} = 244\,8501.730(1) + 2.396\,30(6) \times E. \quad (1)$$

During the spectroscopic observing sessions, a limited number of photometric observations covering the phase intervals $\phi \sim 0.45$–0.6 and 0.9–0.15 were obtained in the Johnson B band using the SBIG ST-9 CCD camera attached to the 0.6-m Optical Craftsman (OC) telescope of MJUO. MAXIMDL[1] software has been used for the reduction of the CCD data. Unfortunately, the quality of photometric observations is not good enough to be used in a light-curve analysis. Nevertheless, two times of minima, $2453\,974.9159 \pm 10$ HJD for primary and $2453\,992.8900 \pm 9$ HJD for the secondary minimum, were obtained. The times of minima have been calculated according

[1] http://www.cyanogen.com

Downloaded from https://academic.oup.com/mnras/article/382/2/609/1028017 by Akdeniz University user on 20 September 2021

Table 1. Radial velocities of η Mus-A obtained by the Fourier disentangling of all orders listed in Table 3. The V_γ velocity obtained by the cross-correlation technique is added to all velocities. The observations of η Mus-B are marked by the superscript [1] in the second column (HJD). The blank line separates the observations made with the SITe and the SI600s detectors.

No	HJD −240 0000	Date	UT	Phase ϕ	RV_1 (km s^{-1})	eRV_1 (km s^{-1})	RV_2 (km s^{-1})	eRV_2 (km s^{-1})
1	53872.88280	2006.05.17	09:11:14	0.421	−43.95	0.29	93.06	0.23
2	53872.98030		11:31:38	0.461	−8.74	1.24	59.00	1.35
3	53872.98690		11:41:08	0.464	−6.98	0.30	56.08	0.28
4	53873.07270		13:44:41	0.500	25.38	0.30	–	–
5	53873.14470		15:28:22	0.530	52.48	0.45	−5.53	4.39
6	53873.14860		15:33:59	0.532	54.01	0.30	−4.92	0.32
7	53873.80060	2006.05.18	07:12:52	0.804	161.59	0.30	−112.50	0.30
8	53873.80460		07:18:37	0.805	161.00	0.20	−112.75	1.98
9	53873.82500		07:48:00	0.814	158.20	0.31	−109.12	0.30
10	53873.82920		07:54:03	0.816	156.64	1.81	−108.98	1.42
11	53873.86130		08:40:16	0.829	152.79	1.36	−104.16	2.43
12	53873.86510		08:45:45	0.831	149.80	2.06	−102.89	3.36
13	53873.92760		10:15:45	0.857	138.16	0.34	−89.07	0.32
14	53873.93250		10:22:48	0.859	136.98	0.34	−87.89	0.32
15	53874.03110		12:44:47	0.900	109.61	0.35	−60.52	0.32
16	53874.03710		12:53:25	0.903	107.32	0.90	−61.36	6.12
17	53874.07190		13:43:32	0.917	96.50	0.34	−47.41	0.31
18	53874.07670		13:50:27	0.919	94.88	0.34	−45.79	0.31
19	53874.12740		15:03:27	0.940	77.57	0.69	−27.92	0.64
20	53874.13200		15:10:05	0.942	75.72	0.33	−26.62	0.30
21	53874.19000		16:33:36	0.966	54.42	0.32	−5.32	0.30
22	53874.19400		16:34:11	0.968	52.93	0.32	−3.84	0.30
23	53874.24470		17:52:22	0.989	34.60	2.16	16.32	1.94
24	53874.24910		17:58:42	0.991	32.02	0.31	17.07	0.30
25	53874.78800	2006.05.19	06:54:43	0.216	−117.76	0.26	166.87	0.33
26	53874.79210		07:00:37	0.218	−118.07	0.25	167.18	0.32
27	53874.83840		08:07:18	0.237	−120.43	0.23	169.55	0.29
28	53874.84260		08:13:21	0.239	−120.96	1.00	169.48	0.53
29	53874.89430		09:27:48	0.260	−120.44	0.20	169.55	0.24
30	53874.89910		09:34:42	0.262	−120.30	0.20	169.41	0.24
31	53874.93170		10:21:39	0.276	−118.70	0.19	167.82	0.21
32	53874.93560		10:27:16	0.277	−118.43	0.18	167.11	1.08
33	53874.97970		11:30:46	0.296	−117.43	2.83	165.69	2.28
34	53874.98370		11:36:32	0.298	−115.80	2.51	163.25	3.35
35	53875.02470		12:35:34	0.315	−107.97	1.30	159.49	4.20
36	53875.07990		13:55:03	0.338	−99.39	1.68	146.84	2.10
37	53875.08560		14:03:16	0.340	−97.53	0.21	146.64	0.15
38	53875.12900		15:05:46	0.358	−87.79	0.22	136.90	0.16
39	53875.18970		16:33:10	0.383	−71.80	0.25	120.91	0.18
40	53875.19510		16:40:57	0.386	−70.24	0.26	119.35	0.18
41	53876.01470	2006.05.20	12:21:10	0.728	168.55	0.18	−119.46	0.25
42	53876.07080		13:41:57	0.751	169.92	0.21	−120.83	0.26
43	53876.09540		14:17:23	0.761	170.00	1.14	−120.00	1.07
44	53966.81020	2006.08.19	07:26:41	0.617	123.03	1.30	−73.82	0.98
45	53966.82510[1]		07:48:09	–	–	–	–	–
46	53966.90400		09:41:46	0.656	146.25	1.55	−97.02	1.16
47	53966.96610		11:11:11	0.682	157.67	1.17	−108.42	0.72
48	53967.79300	2006.08.20	07:01:55	0.027	−1.40	0.95	50.47	1.07
49	53967.88610		09:15:59	0.066	−35.45	1.41	84.48	1.47
50	53967.95960		11:01:49	0.097	−59.86	0.94	108.87	0.97
51	53985.88260	2006.09.07	09:10:57	0.576	92.46	1.35	−43.28	1.06
52	53985.89350[1]		09:26:41	–	–	–	–	–

to Kwee–van Woerden method (Kwee & van Woerden 1956). These minima times, including the *Hipparcos* time of minimum (Table 2) and the conjunction times obtained from spectroscopic data (see Section 3.1), have been used in refining the orbital period of the η Mus-A system. The updated light elements and their rms errors have been calculated by the least-squares method as

$$\mathrm{HJD} = 245\,3974.9160(9) + 2.396\,3161(9) \times E. \quad (2)$$

3 RADIAL VELOCITIES

The RV measurements have been performed on the wavelength-calibrated, normalized spectra after removing the telluric lines using

Downloaded from https://academic.oup.com/mnras/article/382/2/609/1028017 by Akdeniz University user on 20 September 2021

Table 2. Available times of minima for η Mus-A.

HJD −240 0000	Error	Filter	Reference
48501.7300	0.0010	H_p	*Hipparcos*
53874.2690	0.0007	Sp	Present study
53974.9159	0.0010	B	Present study
53992.8900	0.0009	B	Present study

the two different techniques, cross-correlation and Fourier disentangling (KOREL). The two independent techniques are especially useful for inspecting the consistency of the measurements.

3.1 Method of cross-correlations

A common problem of hot star spectra is the limited number of photospheric lines available for RV measurements. The echelle orders and possible lines available for RV measurements are listed in Table 3. Unfortunately, some of the lines are too weak to permit reliable RV measurements. The lines which are used are marked with an 'X' (Column 4 of Table 3).

HR 7773 was chosen as B9IV type RV standard and was observed twice in the first observing session, with same instrument settings and a S/N of ≈180 in the 550-nm wavelength region. The RV of HR 7773 is given to be -1.02 km s^{-1} by Fekel (1999). A Gaussian was fitted to individual line profiles (Si II 6371, He I 5875, Ne I 6316, Cr II 5313, Fe I 5169, Mg I 5172, Mg I 5183, Fe II 5018, Si II 5041, Fe II 4583, Al II 4588, W I 4549, Cr II 4558) of HR 7773 to check its catalogue velocity by SPLOT task in IRAF.[2] The reference wavelengths are from the National Institute of Standards and Technology (NIST) data base. The resulting RV of HR 7773 is -1.06 ± 1.10 km s^{-1}, which is in very good agreement with its catalogue velocity. The uncertainty of 1.10 km s^{-1} is the standard deviation from all RV measurements over all lines.

After confirming the reliability of the wavelength calibration, the cross-correlation procedure has been performed and a Gaussian profile is fitted to the central part of the cross-correlation function (CCF) with the FXCOR task in IRAF to derive the RV. When the spectral lines of the components are heavily blended, the CCFs were represented by two Gaussian profiles using the *deblend* option of the FXCOR task. Heliocentric corrections have been applied to the RVs and the mid-exposure times.

With the preliminary RVs obtained from the cross-correlation techniques, orbital solutions were obtained by least-squares fitting of theoretical RV curves to the data of each order independently (Fig. 1). The orbital period of 2.3963 d (equation 1) was kept fixed, while the eccentricity e, longitude of periastron ω, velocity semi-amplitudes $K_{1,2}$, systemic velocity V_γ and conjunction time (starting from 2453 874.2491) have been converged in the least-squares solution. The six conjunction times obtained from different spectral orders were averaged and used with the three photometric times of minima listed in Table 2 to refine the orbital period to the value given in equation (2).

A second stage of orbital fitting was performed with this refined period and assuming a circular orbit (Table 4), since the eccentricity never deviated significantly from zero.

[2] IRAF is distributed by the National Optical Astronomy Observatories, which is operated by the Association of Universities for Research in Astronomy, Inc. (AURA) under cooperative agreement with the National Science Foundation.

The scatter of the data from the spectral orders 113 and 125 around the RV curves (Fig. 1) is relatively higher than those from the redder orders (see Table 4). The scatter in the solution from the order 113 is probably due to the blending of the Fe II 5018 line with nearby weak lines in the RV-standard star spectrum, while for order 125 the weakness of the photospheric lines is the main cause. A principal reason for the larger scatter in the blue spectral orders could simply be larger noise relative to the depth of the lines. An empirical estimate according to the standard deviation from the theoretical RV curves indicates that a typical error of a measured RV is 1.5 km s^{-1}, which is slightly less accurate than the error in RV of HR 7773 due to slightly lower S/N of η Mus-A spectra.

The systemic velocity was obtained by averaging converged values of V_γ at spectral orders in Table 4, except the orders 113 and 125 because they are the least reliable orders. Finally, a systemic velocity $V_\gamma = 24.55 \pm 1.85$ km s^{-1} is adopted for η Mus-A binary system. As was done for the systemic velocity, the other orbital parameters in Table 4 have been averaged and the averaged values have been adopted and used as input parameters for KOREL solutions.

3.2 Solution with spectral disentangling (KOREL)

The spectra of η Mus-A were also analysed using the new version of the code KOREL, i.e. by the method of Fourier disentangling (Hadrava 1995, 2004), which directly yields the orbital parameters and decomposed spectra of the component stars. The KOREL code was applied with the orbital parameters as determined with the cross-correlation technique as input parameters. Without the need for template spectra, the seven spectra obtained with the SI600s detector, and more echelle orders, can be included in the spectral disentangling analysis.

Lines in the echelle orders (Table 3) have been disentangled independently. During the KOREL solutions, only the updated light elements, the conjunction time T_0 and the orbital period P given in equation (2) were fixed, so that the eccentricity e, longitude of periastron w, and the RV semi-amplitudes K_1 and K_2 were the parameters iterated. KOREL does not derive the systemic velocity, but it measures the RVs of each component relative to the disentangled spectra where the systemic velocity is retained.

KOREL may be used assuming a pre-determined time-dependent light dilution for the lines of both components, or treating light dilution as a free parameter. Since a preliminary orbital solution was available to us from the cross-correlation analysis, KOREL was left free to assign light dilution to the lines of the partially eclipsed component.

In the left-hand panels of Figs 2–4, only three of nine spectral regions of η Mus-A are displayed. The 43 spectra in the region of H$_\beta$ (Fig. 2) are shown as superimposed on the KOREL solutions. Disentangled H$_\beta$ lines of primary and secondary are displayed below the spectra. Similarly, the star spectra and KOREL fits as superimposed for He I 5875 Å are shown in the left-hand panel of Fig. 3. Among the nine orders only the order 97 contains notable telluric lines. Therefore, telluric lines are disentangled only for this order and displayed below the disentangled He I 5875 Å lines in the left-hand panel of Fig. 3. Containing He I 4471 and Mg II 4481 Å lines in the spectral order 127, Fig. 4 shows the seven spectra taken in the second observing session, which were also analysed by KOREL in the same fashion.

On the right-hand panels of Figs 2–4, the O–C (star spectra minus KOREL fits) residuals are displayed. Four spectra fall within the eclipses. The O–C residuals of these spectra are indicated by thicker lines in the right-hand panels of those figures. It is clear that there is

Downloaded from https://academic.oup.com/mnras/article/382/2/609/1028017 by Akdeniz University user on 20 September 2021

Table 3. Spectral order and stellar lines considered in this study. The rest wavelengths are from the NIST data base. The S/N refers to the continuum.

Order no.	Wavelength region	Line		Mean S/N	Remarks
85	6665–6713	6678.15 (He I)	X	140	Relatively weak, not available in the template spectrum.
89	6366–6312	6371.36 (Si II)		135	Relatively strong, available in the template spectrum.
97	5841–5883	5875.62 (He I)	X	130	Relatively strong. Telluric lines are clearly visible. Badly disturbed by telluric lines of H_2O when shifted to longer wavelength.
107	5296–5334	5316.80 (Ne I)	X	130	Weak.
		5313.56 (Cr II)			Weak, sometimes lost in noise.
110	5151–5188	5183.60 (Fe II)		135	Weak.
		5172.68 (Mg I)	X		Weak, sometimes lost in noise and may not be trusted.
		5169.03 (Fe I)			Weak, sometimes lost in noise and may not be trusted.
		5167.32 (Mg I)			Weak, sometimes lost in noise and may not be trusted.
113	5015–5051	5018.43 (Fe II)	X	134	Relatively strong, however, close to the edge of the order.
		5041.03 (Si II)	X		Weaker than Fe II.
117	4843–4878	4861.33 (H_β)		120	Component stars can easily be distinguished.
124	4570–4603	4583.83 (Fe II)		90	Weak.
		4588.19 (Al II)			Weak.
125	4534–4566	4549.51 (W I)	X	90	Weak.
		4558.66 (Cr II)			Weak.

no systematic difference from the other residuals which are taken at out-of-eclipse phases. So, it is understood that KOREL automatically handles line strength ratios during the eclipses.

We use the KOREL utility to derive RVs for the components by cross-correlation of the disentangled component spectra with the observed spectra for later combination of spectroscopic and photometric data in one analysis. These RVs are relative to the systemic velocity, the value of which was added as measured earlier by cross-correlation with a template spectrum. The finalized RVs and their residuals from the orbital solutions are given in Table 1.

Analysing all spectra, KOREL finds orbital parameters together with their standard errors. The nine spectral orders were analysed independently. The orbital parameters from the nine orbital solutions are averaged and adopted. The adopted orbital parameters of η Mus-A are given in Table 5. Although a zero eccentricity was used as an input, independent KOREL solutions all gave a very small orbital eccentricity. Therefore, we believe the eccentricity in Table 5 must be real although it is very small.

4 SIMULTANEOUS LIGHT AND RADIAL VELOCITY SOLUTIONS

The *Hipparcos* photometry and long-term *uvb* and *y*-band photometry (LTPV) by Manfroid et al. (1991) and Sterken et al. (1993) are available from the *Hipparcos* web page[3] and CDS,[4] respectively. Recent *uvby* observations of η Mus-A between 2003 March and May were provided by Hensberge (private communication). Those photometric data were considered in a combined analysis of photometry and spectroscopy. Among the photometric data sets, those of Hensberge (private communication) are relatively more precise and give more reliable light-curve solutions. Therefore, the precision of our light-curve solutions is mainly based on the photometric data by Hensberge (private communication).

The reported $B - V$ colour (-0.09) of η Mus-A by Slawson et al. (1992) is consistent with the B8 V spectral type given in the SIMBAD data base. In order to find the interstellar reddening towards the η Mus-A system, we have used the Q-method of Johnson & Morgan (1953). Using $U - B = -0.36$ and $B - V = -0.09$ colours from Slawson et al. (1992), the Q-parameter is found to be $Q = -0.295$. The Q-method gave an unreddened colour $(B - V)_0 = -0.098$. Consequently, the colour excesses towards η Mus-A are $E(B - V) = 0.008, E(U - B) = 0.006$ and extinction $A_v = 3.1\ E(B - V) = 0.025$ mag. A temperature of 12 700 K corresponds to the unreddened colour of η Mus-A according to the calibration tables of Budding & Demircan (2007).

With the temperature of the primary star fixed from its colours, we proceed with the simultaneous solution of the light and RV curves. The model parameters are adjusted using the light and RV curve analysis code Wilson–Devinney (WD) (Wilson & Devinney 1971; Wilson 1994). The PHOEBE package tool (Prša & Zwitter 2005) has been used for the construction of light-curve and differential-correction fits. Gravity darkening exponents $g_1 = g_2 = 1$ and bolometric albedos $A_1 = A_2 = 1$ were set for radiative envelopes. Logarithmic limb-darkening law was used at each iteration step. Limb-darkening coefficients for Strömgren bands and the *Hipparcos* photometric (H_p) band were taken from van Hamme (1993). The resulting model parameters of simultaneous solutions are given in Table 6 and theoretical light and RV curves fitted to observational data are shown in Fig. 5. The combined solution converged to a circular orbit, indicating that the small eccentricity found by KOREL is probably spurious.

The visual companion η Mus-B is too distant to affect the photometry or spectroscopy. Part of the light of η Mus-C must have entered the slit, but the star is cool and red. Hubrig et al. (2001) estimate its contribution in J(1250 nm), H(1620 nm) and K(2200 nm) as 0.8, 1.5 and 4.5 per cent, respectively, such that no significant contamination with light of the C component is expected in the photometric light curves.

5 MODEL ATMOSPHERE APPLICATIONS

We used the KOREL program primarily to determine the RVs of η Mus-A. In addition, the disentangled spectra of the components

[3] http://www.rssd.esa.int/Hipparcos/EpochPhot.html
[4] http://cdsweb.u-strasbg.fr/

Downloaded from https://academic.oup.com/mnras/article/382/2/609/1028017 by Akdeniz University user on 20 September 2021

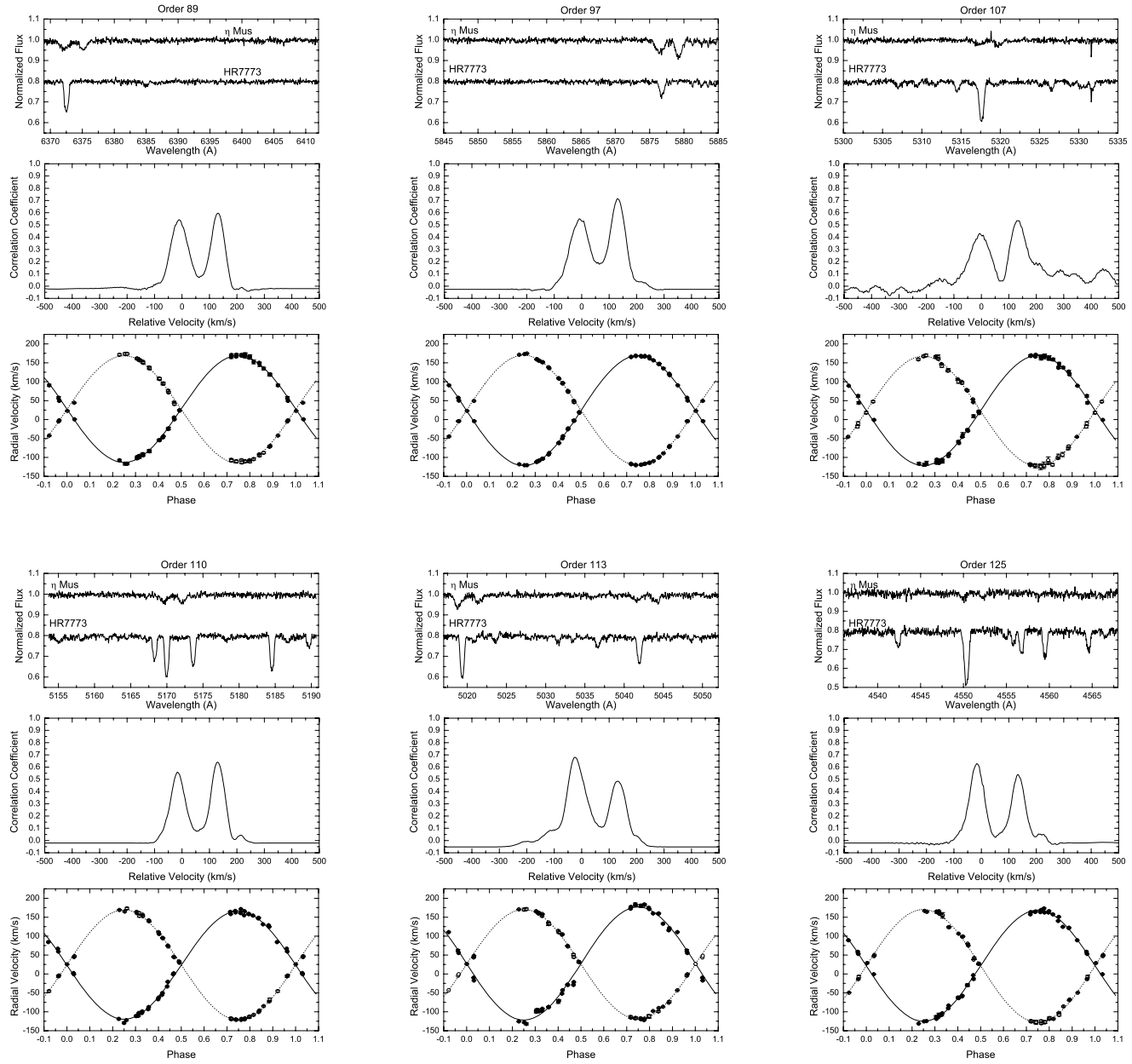


Figure 1. Spectral orders (indicated at the top of each panel) selected for cross-correlation. Panels contain η Mus-A and template spectra (top), CCF (middle) and radial velocities with their orbital solution (bottom).

Table 4. Orbital solutions from the cross-correlation of spectral orders 89, 97, 107, 110, 113 and 125.

Parameter/order	89	97	107	110	113	125
$V_{\gamma 1}$ (km s^{-1})	26.50(0.71)	24.46(0.35)	22.19(0.71)	24.08(0.51)	25.59(0.68)	21.40(0.88)
$V_{\gamma 2}$ (km s^{-1})	28.03(0.56)	23.80(0.30)	24.04(0.78)	23.35(0.78)	26.95(1.56)	21.85(0.92)
K_1 (km s^{-1})	141.87(0.88)	145.58(0.45)	145.17(0.90)	145.20(0.67)	144.64(0.90)	148.99(1.33)
K_2 (km s^{-1})	141.36(0.73)	145.29(1.00)	145.36(1.01)	143.03(0.65)	150.91(4.01)	146.66(1.35)
T_0 −2453 874	0.2694(0.0004)	0.2691(0.0004)	0.2690(0.0004)	0.2688(0.0005)	0.2702(0.0020)	0.2675(0.0020)
P (d)	2.396 3161[a]	2.396 3161[a]	2.396 3161[a]	2.396 3161[a]	2.396 3161[a]	2.396 3161[a]
e	0.0[a]	0.0[a]	0.0[a]	0.0[a]	0.0[a]	0.0[a]
$w(\circ)$	90.0[a]	90.0[a]	90.0[a]	90.0[a]	90.0[a]	90.0[a]
$q(K_1/K_2)$	1.004(1)	1.002(5)	1.001(1)	0.999(2)	0.96(4)	1.016(4)

[a]Parameters fixed during the solutions.

Downloaded from https://academic.oup.com/mnras/article/382/2/609/1028017 by Akdeniz University user on 20 September 2021

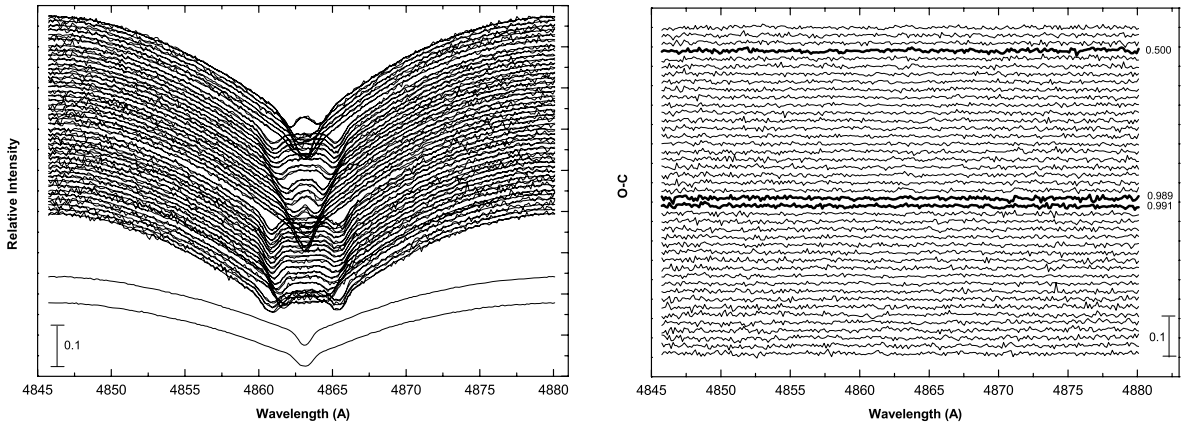


Figure 2. Left-hand panel: the 43 spectra in the region of H_β. Stellar spectra and KOREL fits are superimposed. The disentangled lines of primary and secondary are shown below the fits. Right-hand panel: the O–C residuals from the fits.

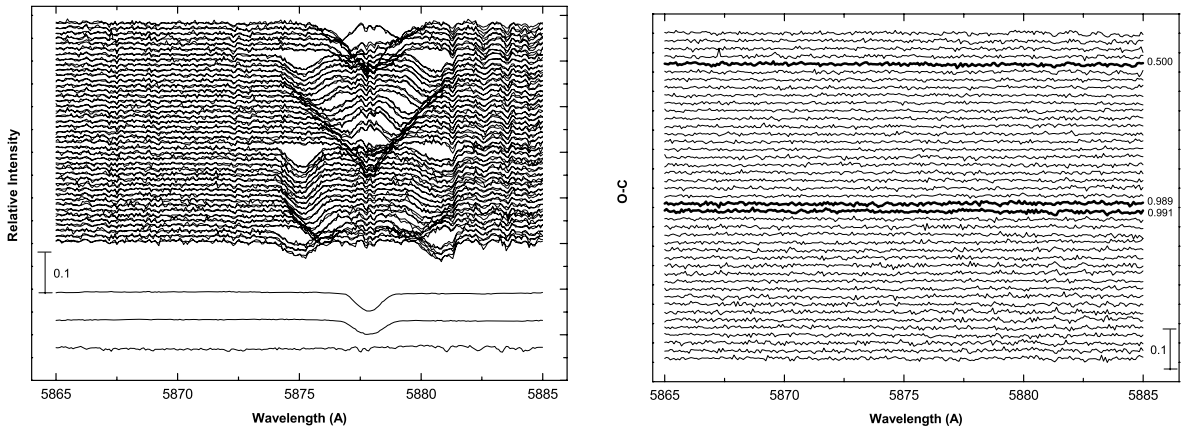


Figure 3. Left-hand panel: the 43 spectra in the region of He I 5875 Å. Stellar spectra and KOREL fits are superimposed. The disentangled lines of primary and secondary and disentangled telluric lines are below the fits. Right-hand panel: the O–C residuals from the fits.

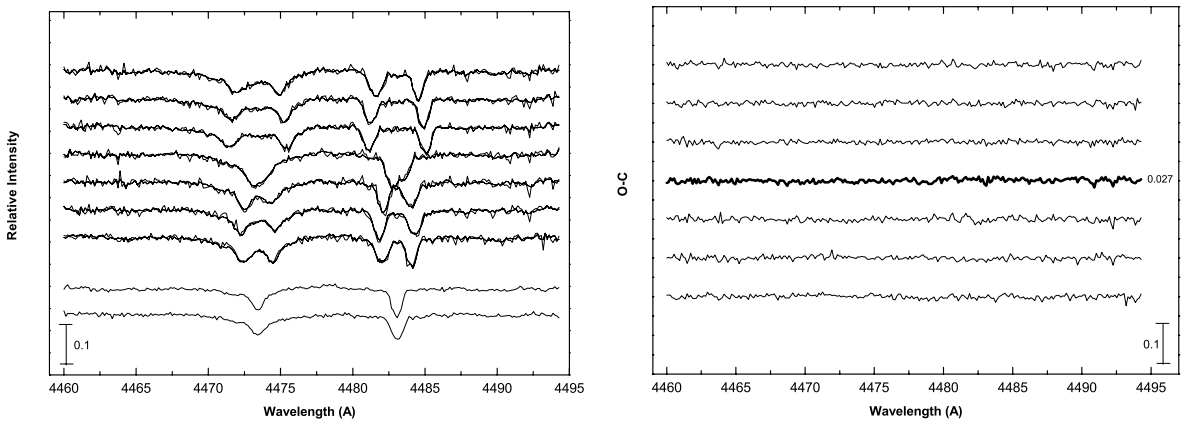


Figure 4. Left-hand panel: the seven spectra in the region of He I 4471 Å and Mg II 4481 Å lines taken in the second observing session. Stellar spectra and KOREL fits are superimposed. The disentangled lines of primary and secondary are below. Right-hand panel: the O–C residuals from the fits.

can be analysed with model atmosphere techniques (see e.g. Hensberge, Pavlovski & Verschueren 2000; Fitzpatrick et al. 2003).

Before doing this, disentangled lines must be renormalized. If S_k is the normalized intrinsic spectrum of the kth component where $k = 1, 2$, S_k can be related to the disentangled spectra (A_k) as

$$A_k = f_k S_k + (1 - f_k), \tag{3}$$

where f_k is the light contribution of the kth component and $(1 - f_k)$ represents the continuum contribution of the other star. The value of f_k is available through light-curve analysis as 51 and 49 per cent

Downloaded from https://academic.oup.com/mnras/article/382/2/609/1028017 by Akdeniz University user on 20 September 2021

Table 5. Spectroscopic orbital parameters of η Mus-A according to KOREL solutions.

Parameter	Values
P (d)	2.396 316 11
T_0	53 974.9160
e	0.0016 ± 0.0009
ω	$90\overset{\circ}{.}3 \pm 0.1$
K_1 (km s^{-1})	145.35 ± 0.2
K_2 (km s^{-1})	145.38 ± 0.2
q	$1.000 \pm .001$
$m_1 \sin^3 i$ ($M_\odot$)	3.06 ± 0.02
$m_2 \sin^3 i$ ($M_\odot$)	3.05 ± 0.02
$a \sin i$ ($R_\odot$)	13.8 ± 0.4

Table 6. Simultaneous light and RV solution for η Mus-A. The parameters without errors are coupled to the other parameters or fixed.

Parameter	Primary	Secondary
P (d)	2.396 3161	
T_0 (HJD)	2453 974.9160	
$a(R_\odot)$	14.11 ± 0.15	
$q(M_2/M_1)$	0.999 ± 0.001	
V_γ(km s^{-1})	24.46 ± 0.02	
$i(^\circ)$	77.4 ± 0.3	
T(K)	12700	12550 ± 300
Ω_1	7.58 ± 0.20	7.62 ± 0.20
$L_u(L/L_{\rm Total})$	0.517 ± 0.053	0.483 ± 0.052
$L_v(L/L_{\rm Total})$	0.511 ± 0.041	0.489 ± 0.040
$L_b(L/L_{\rm Total})$	0.510 ± 0.040	0.490 ± 0.039
$L_y(L/L_{\rm Total})$	0.509 ± 0.040	0.491 ± 0.039
$L_{H_p}(L/L_{\rm Total})$	0.510 ± 0.042	0.490 ± 0.041
r(mean)	0.152 ± 0.005	0.151 ± 0.004
$g_1 = g_2$	1.00	
$A_1 = A_2$	1.00	
e	0.00	
$F_1 = F_2$	1.00	

from primary and secondary, respectively. Of course, this is valid only for the spectra of out-of-eclipse phases. The light-curve solution indicates that the contributions from components are almost independent of wavelength, which is expected as both components have almost identical effective temperatures. This is not valid for the u band (350 nm), where the light contribution of the primary is relatively larger. However, this wavelength region is not used in the present model atmosphere application.

Assuming solar composition ([M/H] = 0 dex), which is a good approximation for stars in Sco OB (Sartori et al. 2003), and a microturbulent velocity (ζ) of 0 km s^{-1} expected for B-type stars (Smalley 2004), a grid of atmosphere models was calculated using the ATLAS9 code (Kurucz 1993) under Linux. While calculating the model atmospheres, the surface gravities of the components ($\log g_{1,2}$) were fixed at the values derived from simultaneous solutions (Section 4) and listed in Table 7. Synthetic line profiles were produced for He I 5875 and 6678 Å individual spectral lines for primary and secondary components using the SYNTHE code (Kurucz 1993). With equation (3) the synthetic line profiles were re-normalized before comparing them with the disentangled lines. $\chi^2_{\rm min}$ test has been applied to estimate the goodness of the fits. The best-fitting model parameters were obtained with $T_{\rm eff1} = 13\,170 \pm 100$ K, $T_{\rm eff2} = 13\,020 \pm 100$ K, $(v \sin i)_1 = 34 \pm 2$ km s^{-1} and $(v \sin i)_2 = 44 \pm 3$ km s^{-1}.

The goodness of the fit is clear in Fig. 6. Temperatures obtained by line profile fitting seem to be higher than the colour temperatures of component stars. However, light-curve analysis and line profile fitting yield the same temperature difference between them.

The best-fitting position of the synthetic lines implies a centre-of-mass velocity $V_\gamma = 26 \pm 4$ km s^{-1}, in agreement with the more precise value of 24.55 ± 1.85 km s^{-1} obtained by the cross-correlation technique.

Another helium line, at 4471 Å, is available together with the Mg II 4481 Å line. With only seven spectra available in this blue part of the spectrum, artefacts might be expected in the disentangled spectra (e.g. Fitzpatrick et al. 2003). Fig. 7 shows the disentangled spectrum of these lines. As can be seen in Fig. 7, the normalized flux level around the Mg II line is below the continuum level, which suggests an extra absorption line of a fast-rotating additional star. This was also noted by Hensberge et al. (2007) in their spectra; however, a detailed analysis is deferred to a future publication. It is desirable to analyse all available sets of spectra together, using spectral disentangling techniques, in order to confirm or exclude the presence of an additional component.

6 THE VISUAL COMPANION: η MUS-B

η Mus-B is reported as an Ap-type star (Vogt & Faúndez 1979). Lindroos (1985) suggested an A3 V-type with metallic-line behaviour according to the m_0 and c_0 indices based on his Strömgren photometry. The $B - V$ colour given in the SIMBAD data base (0.34 mag) and Strömgren indices of Vogt & Faúndez (1979) for η Mus-B are consistent with the spectral type suggested. Using the statistical relation between Strömgren indices of early A-type stars and spectral type (Gray & Garrison 1987) suggests a similar spectral classification of the A2-3 Va type.

Two spectra of η Mus-B were taken with 20-d interval during the observations of η Mus-A in order to investigate the membership of η Mus-B to LCC OB association. The RVs obtained from those spectra could also be used to investigate whether the A- and B-components are gravitationally bound. Gaussian fits to selected spectral lines yield a RV of 12 ± 1 km s^{-1}, close to the median value of the RVs for LCC members as compiled by de Zeeuw et al. (1999). The proper motion and the distance from the Tycho Catalogue (Høg et al. 1997) were combined with this RV measurement and the velocity components of the Sun with respect to the Local Standard of Rest (LSR), $(u, v, w)_\odot$ = (10.00, 5.25, 7.17) km s^{-1} (Dehnen & Binney 1998) to derive for η Mus-B (u, v, w) = (1.6, −14.8, 2.1) km s^{-1} as space velocity components with propagated errors $du = 1.7$ km s^{-1}, $dv = 1.8$ km s^{-1} and $dw = 1.0$ km s^{-1} with respect to the LSR. These values are in close agreement with the movement of LCC as given in Sartori et al. (2003), $(u, v, w)_{\rm LCC}$ = (1.1, −13.6, 1.1) km s^{-1} with a rms scatter $\sigma_u = 5.8$ km s^{-1}, $\sigma_v = 5.6$ km s^{-1}, $\sigma_w = 2.4$ km s^{-1}. This is a strong indicator of membership of η Mus-B.

Assuming that η Mus-A and η Mus-B are at a similar distance, their angular separation corresponds to 6300 au, where the escape velocity from the A-component ($6.77\,M_\odot$) is about 1.4 km s^{-1}, much smaller than the 13 km s^{-1} difference between the centre-of-mass RV of the close binary and η Mus-B. Therefore, it can be concluded that η Mus-A and -B are not gravitationally bound, given that the close binary does not have an orbit with a semi-amplitude larger than 10 km s^{-1} around a yet undetected companion. At present, there is no sign in favour of such a scenario.

No detectable change in the shape or the central wavelength of lines has been observed between the two spectra of η Mus-B.

Downloaded from https://academic.oup.com/mnras/article/382/2/609/1028017 by Akdeniz University user on 20 September 2021

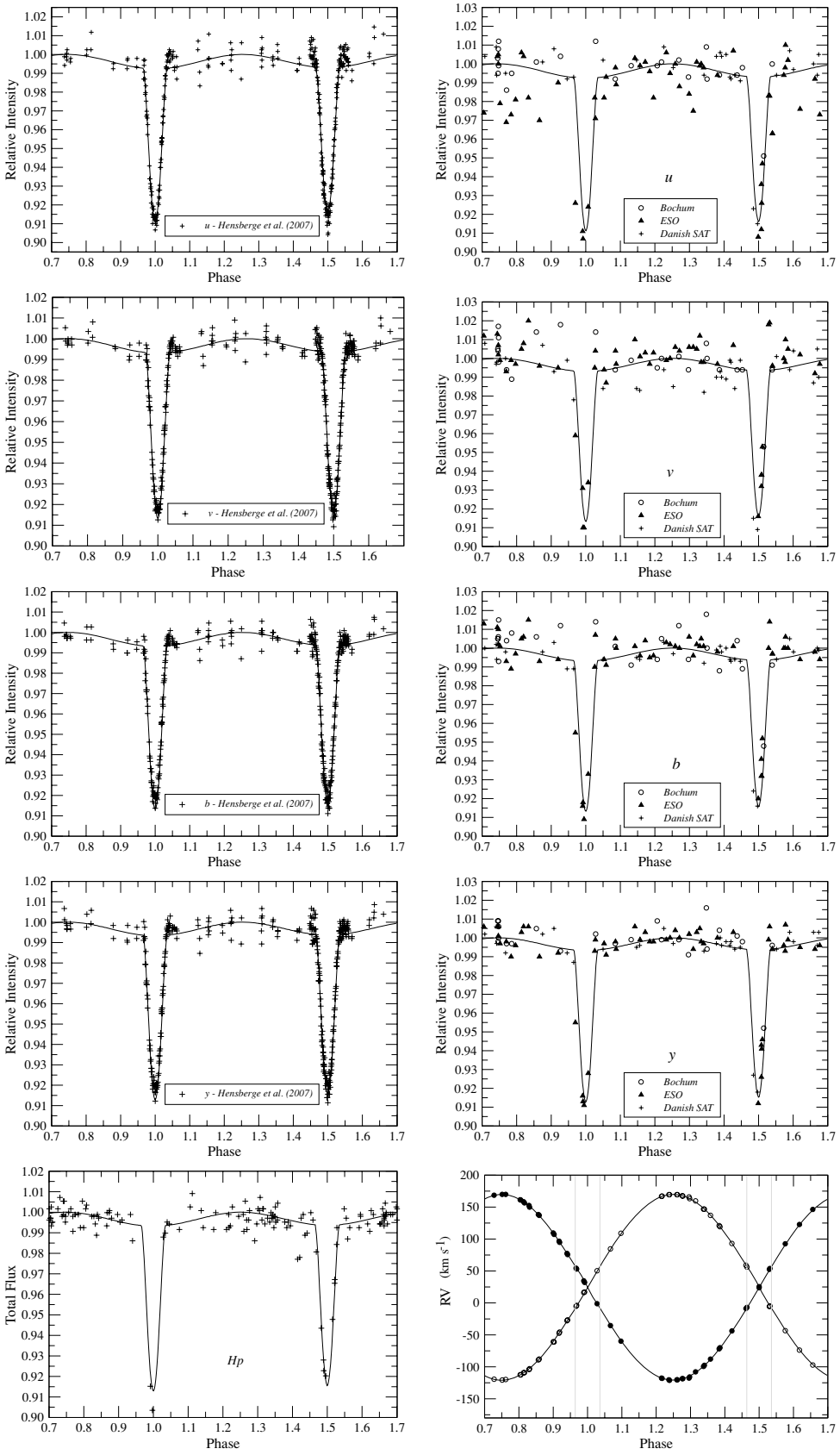


Figure 5. The light and RV solution with the observed data of η Mus-A overplotted. In each panel, photometric band and the source of the data are indicated. LTPV data are shown with three different symbols, each representing different telescope used. In RV solution panel eclipse regions are indicated with vertical lines.

Downloaded from https://academic.oup.com/mnras/article/382/2/609/1028017 by Akdeniz University user on 20 September 2021

Table 7. The absolute dimensions of η Mus-A according to the WD solution in Table 6.

Parameter	Primary	Secondary
$M(M_\odot)$	3.30 ± 0.04	3.29 ± 0.04
$R(R_\odot)$	2.14 ± 0.02	2.13 ± 0.02
T(K)	12700 ± 100	12550 ± 300
$\log L(L_\odot)$	2.03 ± 0.03	2.00 ± 0.03
$a(R_\odot)$	14.11 ± 0.05	
$\log g$ (cgs)	4.293 ± 0.005	4.298 ± 0.005
M_{bol}(mag)	-0.33 ± 0.05	-0.26 ± 0.12
BC	-0.75	-0.66
M_v(mag)	0.42 ± 0.09	0.47 ± 0.09
d (pc)	103 ± 5	

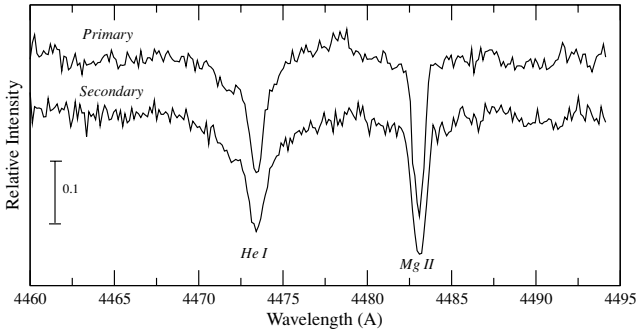


Figure 7. The disentangled He I 4471 Å and Mg II 4481 Å lines of components.

Neither did Vogt & Faúndez (1979) report a photometric variability in their Strömgren photometry. Full width at half-maximum measurements of selected metal lines in η Mus-B spectra imply a projected equatorial rotational velocity of 35 ± 2 km s^{-1}.

7 THE CLOSE-BINARY STELLAR PARAMETERS

The dimensions and fundamental stellar characteristics of the close binary system η Mus-A are summarized in Table 7.

Our simultaneous solutions of photometric and RV curves by the WD method indicate a temperature difference of 150 K between the components whereas the model atmosphere fitting to He I 5875 and 6678 Å lines also confirms it. Although temperatures of both components found by profile fitting, which were found to be 470 K higher than the colour temperatures, indicate a spectral type of B7 V, the physical parameters listed in Table 7 are consistent with the spectral type of B7.5 V for both components. Bolometric corrections corresponding to the adopted temperatures were taken from the table by Budding & Demircan (2007). Absolute luminosities of L_1, L_2 and the distance modulus, which uses the absolute bolometric magnitudes in Table 7, indicate a photometric distance of 103 ± 5 pc for the η Mus-A system. The photometric distance found from the light-curve solutions is small compared to the distance (124 ± 9 pc) corresponding to the trigonometric parallax in the *Hipparcos* catalogue (ESA 1997).

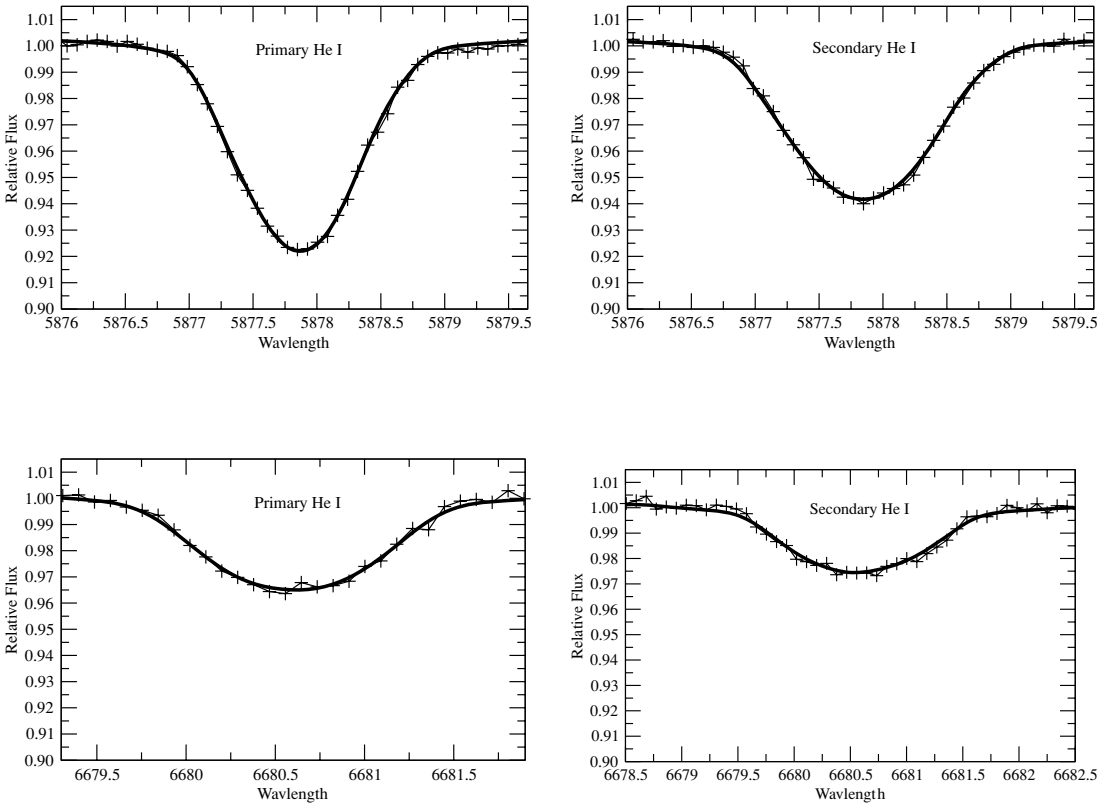


Figure 6. Model atmosphere line profiles (continuous lines) compared to the disentangled (plus signs) He I 5875 Å line of the primary component (top left), and secondary component (top right); and He I 6678 Å line of primary component (middle left), and secondary component (middle right). The synthetic line profiles are normalized using the light contributions of component stars (*see text*).

Downloaded from https://academic.oup.com/mnras/article/382/2/609/1028017 by Akdeniz University user on 20 September 2021

8 DISCUSSION AND CONCLUSIONS

According to the Strömgren and *Hipparcos* photometry and the analysis of high-resolution spectra, η Mus-A is not a single-lined binary as proposed by Buscombe & Morris (1961). It is a double-lined, detached binary with almost equal-mass components in an orbital period of 2.4 d within a visual triple system. The visual component η Mus-B, which is separated 60 arcsec from η Mus-A, is an optical companion, is gravitationally unbound to the close binary. The gravitational binding of the third visual companion η Mus-C, which is the dimmest among the visual components, could not be investigated because no RV data are available, nor is a visual orbit known. It is just discovered by Hubrig et al. (2001) from infrared photometry.

de Zeeuw et al. (1999) have suggested that η Mus-A is a member of LCC OB association with a 60 per cent probability according to their survey. Proper motion, RV and the space velocity vector of η Mus-B confirm the membership of the optical component, but the membership of the close binary needs to be investigated independently.

Combining the *Hipparcos* data and the systemic velocity measured in this paper, the space velocity of η Mus-A with respect to the LSR is $(u, v, w) = (8.8, -25.0, 1.5)$ km s^{-1} with small propagated uncertainties of (1.2, 1.1, 0.3) km s^{-1} and a magnitude $v_s(\sqrt{u^2+v^2+w^2}) = 26.6$km s^{-1}. The magnitude of the corresponding space velocity vector of LCC is 13.7 km s^{-1} with a dispersion of 7.0 km s^{-1} (Sartori et al. 2003). Hence, v_s differs by about 2σ from the LCC mean space velocity magnitude, and the membership of the close binary cannot be proven or disproven in a secure way. Further evidence is needed, based on the age and the chemical composition of the close binary.

In order to investigate the evolutionary stage of η Mus-A and other LCC stars, an HR diagram is presented in Fig. 8 using observational data of stars in LCC which were taken from the compilation of Sartori et al. (2003). The isochrones for main-sequence stars were taken from Bertelli et al. (1994), while the PMS isochrones are taken from Siess, Dufour & Forestini (2000), both for solar chemical composition. The zero-age main-sequence (ZAMS) curve computed by Siess et al. (2000) is also shown. The components of η Mus-A seem to be unevolved from the ZAMS, suggesting an age of 16 $\pm$ 5 Myr, which implies that the system is in the range of the age of 16–20 Myr suggested by Sartori et al. (2003) for the LCC OB association. Unfortunately, a chemical composition test is currently impossible. However, the age of η Mus-A confirms the membership of the system to the LCC association.

A giant star-and-gas complex that is known as the Gould Belt (GB) is a planar distribution of O and B stars in the solar neighbourhood, inclined with respect to the galactic plane with an angle of about 20° (Lesh 1968; Stothers & Frogel 1974; Olano 2001; Pöppel 2001). The centre of the GB is 200 pc away from the Sun in the direction of galactic latitude $l = 200°$ and the semimajor and minor axes of the GB are 500 and 340 pc, respectively (Guillout et al. 1998). The Sun is immersed in the GB system, which is dominated by two prominent nearby OB associations, namely Sco–Cen and Ori OB1 (cf. de Zeeuw et al. 1999). GB contains stars with ages up to 90 Myr (Torra, Fernandez & Figueras 2000). The connection of Sco–Cen with the GB and the derived age of the close binary still leaves an open door for the membership of η Mus-A to the GB.

The fact that the component stars of the close pair Aab rotate with different velocities (34 km s^{-1} for Aa as compared to 44 km s^{-1} for Ab; Section 5) is interesting with respect to the dynamical evolution of binary orbits. Only Ab rotates synchronously with the orbit. The

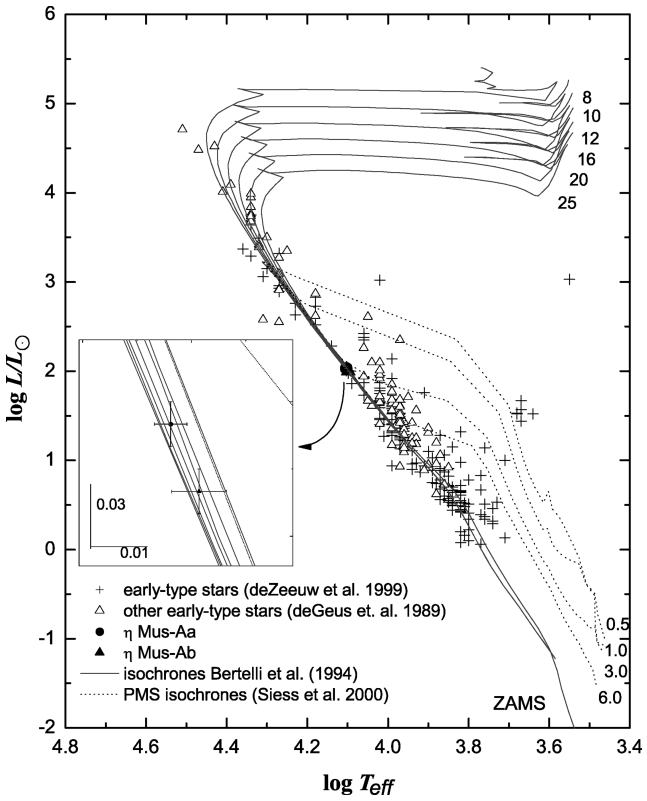


Figure 8. HR diagram of the stars of the LCC OB association. The isochrone ages, in Myr, are indicated by the numbers at the bottom of the PMS isochrone curves, and at the end of the post-main-sequence tracks, for the evolution after the main sequence. Symbols are explained in the lower left corner. For clarity, the location of components of the close binary in HR diagram is displayed in a zoomed panel above the symbol explanations.

sub-synchronous rotation of Aa is a major question. It is known that there are slow-rotating ($v \sin i \sim$ 10–30 km s^{-1}) early-type main-sequence stars which are thought to be the descendants of stars that continued to lose angular momentum through an interaction with an accretion disc until their contraction was nearly completed (Rebull, Wolff & Strom 2004; Herbst & Mundt 2005). Another factor influencing the rotation rates of stars in star formation regions (SFRs) is the accretion rates. Wolff et al. (2007) suggested low accretion rates for low-density SFRs, such as LCC ($\rho = 0.14$ M$_\odot$ pc^{-3}), which will lead to lower initial stellar rotation speeds in the cluster-forming clumps. Hence, one might expect that components of η Mus-A could have started their main-sequence lives as slow rotators.

On the other hand, the second scenario of dynamical evolution is that the components of η Mus-A came to the ZAMS as fast rotators ($v \sin i \sim$ 150–200 km s^{-1}) (see e.g. Gray 1988) and slowed down their velocities because of the tidal forces between the components known as spin orbit coupling. The synchronization time-scale for the component stars of the η Mus-A system is, following Zahn (1977), of the order of 3.5×10^5 yr, which is much smaller than the 16 Myr age estimated from the isochrones and the 16–20 Myr age estimation for the LCC OB region.

A possible explanation could be as follows. Any asynchronous rotation faster than orbital revolution would have implied an inconsistency between the estimated stellar age and the synchronization time-scale. However, a consistent scenario can be established much easier by slower than synchronous rotation. It appears as if η Mus-A system has achieved a synchronization within a time-scale which is

Downloaded from https://academic.oup.com/mnras/article/382/2/609/1028017 by Akdeniz University user on 20 September 2021

obviously smaller than the age of the η Mus-A system. The η Mus-A system is located in a crowded region, that is, stellar encounters are very likely. Stellar encounters may cause a binary to lose considerable amount of orbital angular momentum. Additionally, it is known that the η Mus-A system has a third visual companion 2.71 arcsec away, which is more likely to draw orbital angular momentum with a similar mechanism, as described by Paczyński et al. (2006) for the formation of contact binaries by the three-body orbital evolution.

A stellar encounter may cause a binary orbital period to decrease suddenly if orbital angular momentum is lost from it. Since such an encounter does not draw angular momentum from components but only from the orbit, component stars keep their rotation periods and the system becomes asynchronous again after the encounter due to the decreased orbital period. Obviously, the less massive components have caught up in rotational speed through synchronization but the more massive component needs more time. The very similar mass of the components seems to be against this hypothesis. However, perhaps more than the mass difference, the internal mass distribution of the secondary is different from that in the primary star and helpful for synchronization.

A hypothetical additional wide component, which might produce a faint, wide Mg II line in the spectra, could be relevant to understand the lack of synchronization in the close binary. Therefore, we encourage high signal-to-noise ratio spectroscopy to further investigate the multiplicity of this system.

ACKNOWLEDGMENTS

This study is part of a project carried out in Southern hemisphere which is fully supported by The Scientific & Technological Research Council of Turkey (TUBITAK) under the project code 2214. It is also part of the PhD thesis of VB who would like to specifically thank Professor Ed Budding for his valuable discussions during the preparation of the project, Professor John Hearnshaw for allowing observing time, the Carter Observatory Board for providing an office and the technical staff (Alan Gilmore, Pam Kilmartin, Steven Barlow, Nigel Frost and Paul Tristram) at MJUO for their warm hospitality during his research programme in New Zealand and members of the Physics and Astronomy Department at the University of Canterbury for their warm hospitality. We would like to express our sincere gratitude to the reviewer, Herman Hensberge, for his useful comments which improved the quality of this paper.

REFERENCES

Batten A. H., Fletcher J. M., MacCarthy D. G., 1989, Publ. Dom. Astrophys. Obs., 17, 1
Bertelli G., Bressan A., Chiosi C., Fagotto F., Nasi E., 1994, A&AS, 106, 275
Brown A. G. A., Blaauw A., Hoogerwerf R., de Bruijne J. H. J., de Zeeuw P. T., 1999, in Lada C. J., Kylafis N. D., eds, The Origin of Stars and Planetary Systems. Kluwer Academic Publishers, p. 411
Budding E., Demircan O., 2007, Introduction To Astronomical Photometry, 2nd edn. Cambridge Univ. Press, Cambridge
Buscombe W., Morris P. M., 1961, MNRAS, 123, 183
Campbell L., 1928, Lick Obs. Publ., 16, 195
Crawford D. L., Barnes J. V., Golson J. C., 1970, AJ, 75, 624
Dehnen W., Binney J. J., 1998, MNRAS, 298, 387
de Zeeuw P. T., Hoogerwerf R., de Bruijne J. H. J., Brown A. G. A., Blaauw A., 1999, AJ, 117, 354
Eggen O. J., Lyngå G., 1968, ApJ, 153, 195
ESA, 1997, ESA SP-1200, The Hipparcos Catalogue. ESA Publications Division, Noordwijk
Fekel F. C., 1999, in Hearnshaw J. B., Scarfe C. D., eds, ASP Conf. Ser. Vol. 185, Precise Stellar Radial Velocities. Astron. Soc. Pac., San Francisco, p. 378
Fitzpatrick E. L., Ribas I., Guinan E. F., Maloney F. P., Claret A., 2003, AJ, 587, 685
Guillout P., Sterzik M. F., Schmitt J. H. M. M., Motch C., Neuhäuser R., 1998, A&A, 337, 113
Giuricin G., Mardirossian F., Mezzetti M., 1984, ApJS, 54, 421
Gray D. F., 1988, Lectures on Spectral-Line Analysis: F, G, and K Stars. Arva, Ontario
Gray R. O., Garrison R. F., 1987, ApJS, 65, 581
Hadrava P., 1995, A&AS, 114, 393
Hadrava P., 2004, Publ. Astron. Inst. Cz., 92, 1
Hearnshaw J. B., Barnes S. I., Kershaw G. M., Frost N., Graham G., Ritchie R., Nankivell G. R., 2002, Exp. Astron., 13, 59
Hensberge H., Pavlovski K., Verschueren W., 2000, A&A, 358, 553
Hensberge H. et al., 2003, in Luine L., Gregorio-Hetem J., eds, Astrophys. Space Sci. Library Vol. 299, Open Issues in Local Star Formation. Kluwer, Dordrecht, p. 299
Hensberge H. et al., 2007, MNRAS, 379, 349
Herbst W., Mundt R., 2005, ApJ, 633, 967
Høg E. et al., 1997, A&A, 323, 57
Hubrig S., Mathys G., 1996, A&AS, 120, 457
Hubrig S., Mignant D. Le., North P., Krautter J., 2001, A&A, 372, 152
Johnson H. L., Morgan W. W., 1953, ApJ, 117, 313
Kurucz R. L., 1993, CD-ROM 13, 18, http://kurucz.harward.edu
Kwee K. K., van Woerden H., 1956, Bull. Astron. Inst. Netherlands, 12, 327
Lesh R. J., 1968, ApJS, 17, 371
Lindroos K. P., 1983, A&AS, 51, 161
Lindroos K. P., 1985, A&AS, 60, 183
Manfroid J. et al., 1991, A&AS, 87, 481
Medici A., Hubrig S., 2000, IBVS 4827
Moffat A. F. J., Seggewiss W., 1977, A&A, 54, 607
Olano C. A., 2001, AJ, 121, 295
Paczyński B., Szczygiel D. M., Pilecki B., Pojmanski G., 2006, MNRAS, 368, 1311
Pöppel W. G. L., 2001, in von Hippel T., Simpson C., Manset N., eds, ASP Conf. Ser. Vol. 243, Astrophysical Ages and Time Scales. Astron. Soc. Pac., San Francisco, p. 667
Prśa A., Zwitter T., 2005, ApJ, 628, 426
Rebull L. M., Wolff S. C., Strom S. E., 2004, AJ, 127, 1029
Sartori M. J., Lepine J. R. D., Dias W. S., 2003, A&A, 404, 913
Schilt J., Jackson C., 1949, AJ, 55, 9
Siess L., Dufour E., Forestini M., 2000, A&A, 358, 593
Skuljan J. R., 2004, in Kurtz D. W., Pollard K. R., eds, ASP Conf. Ser. Vol. 310, Variable Stars in the Local Group. Astron. Soc. Pac., San Francisco, p. 575
Skuljan J. R., David J., Hearnshaw J. B., 2004, MNRAS, 352, 975
Slawson R. W., Hill R. J., Landstreet J. D., 1992, ApJS, 82, 117
Smalley B., 2004, in Zverko J., Weiss W. W., Ziznovsky J., Adelman S. J., eds, Proc. IAU Symp. 224, The A-Star Puzzle. Cambridge Univ. Press, Cambridge, p. 131
Stothers R., Frogel J. A., 1974, AJ, 79, 456
Sokolov N. A., 1995, A&AS, 110, 553
Sterken C. et al., 1993, A&AS, 102, 79
Tokovinin A. A., 1997, A&A, 124, 75
Torra J., Fernandez D., Figueras F., 2000, A&A, 359, 82
van Hamme W., 1993, AJ, 106, 2096
van Paradijs J., van Amerongen S., Damen E., van der Woerd H., 1986, A&AS, 63, 71
Vogt N., Faúndez M. A., 1979, A&AS, 36, 477
Wilson R. E., 1994, PASP, 106, 921
Wilson R. E., Devinney E. J., 1971, ApJ, 166, 605
Wolff S. C., Strom S. E., Dror D., Venn K., 2007, AJ, 133, 1092
Zahn J. P., 1977, A&A, 57, 383

This paper has been typeset from a TEX/LATEX file prepared by the author.

Downloaded from https://academic.oup.com/mnras/article/382/2/609/1028017 by Akdeniz University user on 20 September 2021